High-Throughput Glycan Array Screening Reveals Rhamnogalacturonan-I as a Ligand for Arabidopsis Leucine-Rich Repeat Receptor Kinases

Authors:

Du-Hwa Lee[1, 2, §, *], Colin Ruprecht[1, §], Jung-Min Lee[2], Min-Soo Choi[2], Tobias Hrovat[2], Geon Heo[2], Natalie Edelbacher[2], Balaji Enugutti[2], Markus Blaukopf[1], Chung Hyun Cho[2], Ho-Seok Lee[2, 3, 4], Youssef Belkhadir[2, 5], Elwira Smakowska-Luzan[2, 6], Fabian Pfrengle[1, *]

Affiliations:

[1] Department of Natural Sciences and Sustainable Resources, BOKU University, Muthgasse 18, 1190 Vienna, Austria

[2] Gregor Mendel Institute (GMI), Austrian Academy of Sciences, Vienna BioCenter (VBC), Dr. Bohr-Gasse 3, Vienna, Austria

[3] Current address: Department of Biology, Kyung Hee University, 02447 Seoul, Korea

[4] Current address: Center for Genome Engineering, Institute for Basic Science, 34126 Daejeon, Korea

[5] Current address: Douar Ifraden, Residence Taghazout Ocean #13, Taghazout 8000, Morocco

[6] Current address: Wageningen University and Research, Laboratory of Biochemistry, Wageningen, The Netherlands

[§] These authors contributed equally.

* To whom correspondence should be addressed:
duhwa.lee@boku.ac.at, fabian.pfrengle@boku.ac.at

Abstract

The plant cell wall not only serves as a physical barrier against pathogens but, when damaged, also functions as a source of cell wall-derived molecules that play crucial roles in plant immunity as damage-associated molecular patterns (DAMPs). While oligogalacturonides from homogalacturonan are well-studied DAMPs, the immune-signaling potential of other cell wall components remains largely unexplored. Conventional genetic and biochemical approaches aimed at identifying ligand-receptor pairs in plant immunity have been limited by the vast diversity of potential ligand molecules and functional redundancy of putative receptors. Here, we developed a high-throughput screening pipeline that simultaneously examines multiple interactions between plant cell wall-derived glycans and >350 extracellular domains (ECDs) of receptor kinases and receptor like proteins in Arabidopsis, resulting in the screening of >40,000 interactions. We discovered a group of leucine-rich repeat receptor kinases named ARMs (AWARENESS of RG-I MAINTENANCES) that interact with rhamnogalacturonan-I (RG-I), a major component of pectin. RG-I treatment induced pattern-triggered immunity responses, with distinct kinetics compared to oligogalacturonide responses. We identified RG-I oligosaccharide structures required for interaction with ARM receptors and immune activation, and found that ARM receptors are redundantly involved in plant immunity. Thus, our approach provides a powerful platform for discovering glycan-receptor pairs in plants.

Introduction

The cell wall, as the outermost structure, serves as a primary barrier for plant cells against interacting organisms[1]. The plant cell wall contains large amounts of the polysaccharides, including cellulose, hemicellulose, and pectin, which provide structural integrity and support[2]. Due to its outermost nature, the cell wall is the first target to break down during pathogen or pest attacks[3]. In the context of innate immunity, products of cell wall breakdown can be recognized as typical extracellular warning signals[4]. Cell wall components of attacking organisms are categorized as microbe-associated molecular patterns (MAMPs), whereas host cell wall components produced by mechanical forces or digestion of enzymes by attacking organisms are categorized as damage-associated molecular patterns (DAMPs)[5]. Plants have evolved an expanded repertoire of cell surface receptors to respond to such MAMPs/DAMPs[6]. This subset of cell surface receptors is called pattern recognition receptors (PRRs), triggering pattern-triggered immunity (PTI) upon binding these molecular patterns[7]. For example, PRRs of the lysin motif (LysM) family, CHITIN ELICITOR RECEPTOR KINASE 1 (CERK1) and LysM motif receptor kinase 4 and 5 (LYK4 and LYK5) can recognize

the glycan-type MAMP chitohexaose (β-1,4-D-N-acetylglucosamine)$_6$ from fungal pathogens[8-10]. To date, some glycan-type DAMP ligand-receptor pairs have been extensively studied: firstly, Arabidopsis wall-associated kinases 1 and 2 (WAK1 and WAK2) have been shown to interact with the glycan-type DAMP oligogalacturonic acid (α-1,4-oligogalacturonan; OGs) derived from plant pectin, and have been implicated in OGs perception[11,12]. Among OG fragments, those with 10-15 degrees of polymerization ($OG^{DP10-15}$) have been shown to induce the strongest immune responses[13-15]. However, two independent recent studies using a quintuple deletion mutant of WAK1 and its homologs WAK2-5, generated by the clustered regularly interspaced short palindromic repeats (CRISPR)/CRISPR-associated 9 (Cas9) technique, showed no or only minor changes in PTI response to OGs[16,17], suggesting functional redundancy between WAK receptors with WAK-like (WAKL)-family receptors. More recently, PRRs containing leucine-rich-repeat (LRR) and malectin (MAL) domains, namely CELLO-OLIGOMER RECEPTOR KINASE1/IMPAIRED IN GLYCAN PERCEPTION 1, 2, and 4 (CORK1/IGP1-4), have been identified as receptors for cello-oligomers (β-1,4-oligoglucans), such as cellotriose[18,19]. These studies revealed direct binding between CORK1/IGP receptors and cello-oligosaccharides resulting in impaired immune responses in receptor mutants. Given the diversity of glycan compositions in the plant cell wall and the wide range of cell wall-degrading enzymes (CWDEs) secreted by pathogens, an array of cell wall derivatives can be produced as MAMPs/DAMPs during pathogen attack[2,20]. Indeed, a significant number of glycans have been identified to trigger PTI responses, including (arabino-)xylan, mixed linkage glucan (MLG), xyloglucan and mannan oligosaccharides[4,21-27]. While putative receptors for some of these glycan ligands have been reported, substantial opportunity remains for discovering novel glycan ligands that trigger PTI responses as well as investigating their ligand specificities and the molecular mechanisms resulting upon ligand perception.

The general responses of PTIs, even when activated by different ligands, share key conceptual similarities[7]. Upon detecting MAMPs/DAMPs, the corresponding receptor kinases (RKs) or associated RKs are activated and initiate downstream signal transduction pathways. Key features of PTI include the activation of ion channels, production of reactive oxygen intermediates (ROIs), activation of defense-related mitogen-activated protein kinases (MAPKs) cascades, and extensive transcriptomic changes[28,29]. Prolonged MAMPs/DAMPs exposure leads to long-term trade-offs between resource allocation for growth and immune responses, ultimately leading to growth inhibition[30-32]. To date, various approaches have been employed to identify receptor-ligand relationships. Forward genetic screens using chemical mutagens such as ethyl methanesulfonate (EMS) have been one of the most successful strategies, relying

on monitoring PTI response readouts after known MAMP/DAMP molecules treatment[18,19,33,34]. However, many PRRs have been reported to have redundant functions[35-37], demonstrating the limitations of these forward genetic approaches in determining multiple receptor-ligand relationships.

In this study, we developed a high-throughput screening pipeline to examine the multiple interactions between cell wall-derived glycans and a protein expression library of extracellular domains (ECDs) from RKs and receptor-like proteins (RLPs) in Arabidopsis (Fig. 1A). Using this pipeline, we identified five ECDs of RKs that interact with rhamnogalacturonan-I (RG-I), a component of pectin. These receptors, named AWARENESS of RG-I MAINTENANCES (ARMs), bind RG-I polysaccharides as well as defined RG-I oligosaccharides either purified from natural sources or synthesized and are required for resistance to pathogenic bacterial infection.

Results

We previously established an Arabidopsis LRR-RK network using about 200 ECDs in a recombinant protein expression library for *Drosophila* Schneider S2 cells[38]. We have since expanded this library to encompass 422 ECDs from RKs and RLPs in the Arabidopsis genome, covering a broader range of receptor classes (Fig. 1B and Supplementary Fig. 1). 357 of these proteins, for which expression levels and estimated sizes were confirmed using immunoblotting assays (Supplementary Fig. 2, Supplementary Table 1), were subsequently used in binding assays with a glycan array populated with about 100 synthetic plant oligosaccharides and 16 commercially available plant polysaccharides, resulting in the determination of 43,554 interactions. (Fig. 1C). The chemically synthesized oligosaccharides include arabinoxylan, type I and type II arabinogalactans, xyloglucan, rhamnogalacturonan-I, and mixed-linkage glucan oligosaccharides, representing fragments of natural hemicelluloses and pectins, as well as hydroxyproline-rich glycoproteins (Supplementary Fig. 3)[39,40]. To ensure that receptor-glycan interactions can be detected using the glycan array assay, we performed proof-of-concept binding studies using LYK5^{ECD} and CERK1^{ECD}. Both proteins bound to chitohexose and chitosan polysaccharides on the array, with LYK5^{ECD} interacting stronger, particularly to chitosan compared to CERK1^{ECD} (Fig. 1D, Supplementary Fig. 4A, and Supplementary Table 2). Besides LYK5^{ECD} and CERK1^{ECD}, which were used as positive controls, only five ECDs from a subfamily of LRR-RKs interacted with glycans on the array. All five ECDs bound the polysaccharides rhamnogalacturonan-I (RG-I), arabinan (ARAn), and galactan (GALn) (Fig. 1D and Supplementary Table 2). The backbone of RG-I consists of

alternating units of D-galacturonic acid (GalA) and L-rhamnose (Rha) [4)-α-D-GalA-(1,2)-α-L-Rha-(1]$_n$, with the Rha residues partially being substituted by side chains such as galactan (GALn; β-1,4-galactan), arabinan (ARAn; α-1,5-arabinan), and arabinogalactan (β-1,4-galactan with α-1,5-arabinan branches) (Fig. 1E). The three bound commercially available polysaccharides were originally purified from plant pectin and might thus contain different pectic polysaccharides. To test for the presence of RG-I in the GALn and ARAn samples, we used the monoclonal antibody INRA-RU2, which specifically binds to the RG-I backbone[40,41]. INRA-RU2 bound in addition to RG-I also to the GALn and ARAn samples on the array, indicating the presence of RG-I in these samples (Fig. 1F). To determine if these ECDs bind to the RG-I backbone, we selected one positive hit (AT1G10850) and performed on-array digestion using an endo-RG-I hydrolase. We found that the binding of this ECD was abolished when RG-I was digested, indicating that the RG-I backbone structure is essential for binding. We therefore named these five receptors AWARENESS of RG-I MAINTENANCES (ARMs).

Based on ECD protein sequence similarity analysis, the five ARM receptors were distributed across 3 different clades, which we named ARM1, ARM2, and ARM3 with increasing numbers of LRRs and ECD sizes, respectively (Fig. 2A and Supplementary Fig. 4B). Within these clades, we found pairs of positive hits that were closest homologs to each other in the ARM1 and ARM3 clades, which we designated as ARM1a (AT1G10850)/ARM1b (AT1G60630) and ARM3a (AT2G16250)/ARM3b (AT4G39270), respectively. The ARM2 clade contained only one positive hit, AT3G56100, which we designated as ARM2a. Although its closest homolog AT3G51740 did not show positive interactions in our screening (Supplementary Fig. 4A), we designated it as ARM2b and included it in further detailed interaction assays. To quantify the interaction between ARM^{ECD}s and RG-I polysaccharides, we purified the ARM^{ECD}s (Supplementary Fig. 4C) and performed microscale thermophoresis (MST) assays. Due to the heterogeneous nature of polysaccharides, we determined the half-maximal effective concentration (EC50) values rather than dissociation constants (Kd). The five ARM^{ECD}s that showed positive interactions with RG-I polysaccharides in the screening exhibited EC50 values ranging from 31.85±6.23 μg/mL (ARM2a^{ECD}) to 70.27±14.09 μg/mL (ARM1b^{ECD}) (Fig. 2B). Interestingly, while ARM2b^{ECD} did not bind to RG-I on the array, it showed interaction with RG-I in MST, albeit with a higher EC50 value of 119.2±22.84 μg/mL (Fig. 2B), indicating a weaker interaction compared to the other ARM^{ECD}s. This result suggests that the protein affinity threshold for binding on the glycan array corresponds to EC50 values between ARM2b^{ECD} and ARM1b^{ECD}, i. e. 70-120 μg/mL. Additionally, we were unable to detect interactions between ARM1a^{ECD} and OG$^{DP10-15}$ or between a randomly selected large

LRR^{ECD} (AT5G14210) and RG-I in the MST assay (Fig. 2C and D), indicating the specificity of the interactions between ARM^{ECD}s and RG-I polysaccharides.

Next, we investigated the potential PTI responses triggered by RG-I treatment. Unlike $OG^{DP10-15}$ treatment, RG-I treatment did not induce acute Ca^{2+} influx (Fig. 3A) or production of ROIs within 120 minutes (Fig. 3B). However, RG-I did induce MAPK activation, similar to that observed with $OG^{DP10-15}$ treatment (Fig. 3C). Polygalacturonan (PGA) treatment, the polysaccharide form of $OG^{DP10-15}$, resulted in weaker MAPK activation compared to RG-I and $OG^{DP10-15}$, while the flagellin fragment flg22, also used as a positive control, induced strong MAPK activation in wild-type plants but not in the flg22 receptor mutant *fls2* (Fig. 3C). Furthermore, RG-I induced stronger MAPK activation compared to GALn and ARAn (Fig. 3D), indicating that the RG-I backbone structure is critical not only for binding to ARMs but also for activating PTI responses. Root growth inhibition was observed in seedlings grown on RG-I-containing media, while no such inhibition was observed in media containing $OG^{DP10-15}$ (Supplementary Fig. 5A). To explore that these hypothetic indications of immune responses are accompanied by gene expression-defined programs, we performed RNA-seq analysis to characterize genome-wide transcriptional changes triggered by RG-I treatment. These changes were compared to those induced by $OG^{DP10-15}$ treatment (Fig. 3E and F)[28]. The repertoire of differentially expressed genes (DEGs) induced by RG-I treatment was similar to that induced by $OG^{DP10-15}$ (Fig. 3E), indicating that RG-I treatment triggered a general gene expression immune response. In particular, the upregulated DEGs following RG-I treatment showed a more pronounced overlap with those upregulated by $OG^{DP10-15}$ treatment compared to the overlap observed among downregulated DEGs. Among the 1,483 upregulated DEGs identified after RG-I treatment (Supplementary Fig. 5B and C), 948 genes (63.9%) overlapped with upregulated DEGs from $OG^{DP10-15}$ treatment across the four analyzed time points, i. e. 30 and 90 minutes for both RG-I and $OG^{DP10-15}$ treatments (Fig. 3F, upper panel). Gene Ontology (GO) analyses of the 303 upregulated DEGs shared between RG-I and $OG^{DP10-15}$ treatment highlighted biological processes related to plant immune responses and defense mechanisms (Fig. 3G and Supplementary Table 3). GO analyses of 488 upregulated DEGs common to RG-I treatments at 30 and 90 minutes also indicated similar biological processes (Supplementary Fig. 5D and Supplementary Table 3). These transcriptomic changes were confirmed by quantitative RT-PCR analysis of the selected PTI marker gene *FLG22-INDUCED RECEPTOR KINASE 1* (*FRK1*) (Supplementary Fig. 5E). Collectively, our results suggest that RG-I treatment induces a range of PTI responses, including MAPK activation and extensive defense-

related transcriptomic changes, similar to those triggered by $OG^{DP10-15}$, but with distinct kinetics in Ca^{2+} influx and ROI production.

To identify the essential structural requirements of RG-I for PTI activation, we performed sequential enzymatic digestion of RG-I polysaccharides to obtain RG-I oligosaccharides (Fig. 4A). First, we trimmed the side chains using galactanase and arabinofuranosidase, then removed the hydrolysis products by dialysis. The trimmed RG-I polysaccharides (RG-I Trim) still induced MAPK activation, supporting our assertion that the RG-I backbone is crucial for PTI activation (Fig. 4B). Next, we hydrolyzed the RG-I backbone using RG-I hydrolase (RG-I Digest) and purified the resulting oligosaccharides to remove proteins and unhydrolyzed polysaccharide (RG-I Oligomix). Both RG-I Digest and RG-I Oligomix induced MAPK activation, demonstrating that the activation was not due to proteinaceous molecules but rather was triggered by the RG-I oligosaccharides themselves. Additionally, when we repeated this procedure with an RG-I lyase, we found that RG-I oligosaccharides generated by either RG-I hydrolase (Hydrolase Oligomix) or RG-I lyase (Lyase Oligomix) induced MAPK activation (Fig. 4C). The hydrolase-generated oligosaccharides were then separated by size and purified by High-performance liquid chromatography (HPLC) using a PGC column to obtain defined oligosaccharides (Supplementary Fig. 6A). We successfully purified specific RG-I oligosaccharides with one or two galactose substitutions on a tetrasaccharide backbone (4+1, 4+2) and two or three galactose substitutions on a hexasaccharide backbone (6+2, 6+3) in sufficient yields for further analysis. The compositions of these oligosaccharides were determined by Matrix-assisted laser desorption ionization-time of flight mass spectrometry (MALDI-TOF-MS) (Supplementary Fig. 6B and C). Nuclear magnetic resonance (NMR) spectroscopy analysis of the 4+2 and 6+2 oligosaccharides revealed that for these two oligosaccharides each rhamnose residue was substituted with no more than one galactose (Fig. 4E and Supplementary Fig. 6D).

Each purified RG-I oligosaccharide induced MAPK activation, with the 6+2 oligosaccharide eliciting the strongest response (Fig. 4D). Next, we performed MST analyses to determine the Kd for interactions between the ARM^{ECD}s and either purified oligosaccharides (4+2, 6+2) or a chemically synthesized unsubstituted RG-I backbone heptasaccharide (7+0) (Fig. 4E-H)[42]. MST analysis revealed that $ARM1a^{ECD}$ showed increasing affinity to oligosaccharides with longer backbones and/or fewer substitutions, based on the calculated Kd values of 4+2 (162.62±135.74 μM), 6+2 (90.18±50.68 μM), and 7+0 (61.26±32.42 μM) oligosaccharides (Fig. 4F). However, the opposite trend was observed for $ARM2a^{ECD}$ and $ARM3a^{ECD}$, which showed decreased affinity for the 7+0 oligosaccharide compared to the 4+2 oligosaccharide

(Fig. 4G and H). Collectively, our results indicate that specific RG-I oligosaccharides can function as immunogenic molecules capable of inducing MAPK activation. Furthermore, our binding studies reveal distinct oligosaccharide preferences among ARM^{ECD}s, while the functional significance of these differential binding patterns requires further investigation.

To investigate the loss-of-function phenotypes of ARMs, we first analyzed single mutants of each ARM gene using either transfer DNA (T-DNA) insertion lines or mutants generated by CRISPR/Cas9 technique (Supplementary Fig. 7). Additionally, we generated high-order mutants including double mutants (*arm1a/1b*, *arm2a/2b*, and *arm3a/3b*) and quadruple mutants (*arm1a/1b/2a/2b, arm1a/1b/3a/3b,* and *arm2a/2b/3a/3b*). However, none of the single, double, or quadruple mutants showed significantly different response to RG-I treatment compared to wild-type, as monitored by both MAPK activation and *FRK1* gene induction, suggesting potential functional redundancy among the ARM proteins in RG-I recognition (Supplementary Figs. 8-11). We further extended our analysis by generating and testing two different sextuple mutants (labeled #13 and #17) lacking all six ARM genes (Fig. 5A). In response to RG-I treatment, the sextuple mutants showed wild-type levels of both MAPK activation and *FRK1* expression (Fig. 5B and Supplementary Fig. 11C). The mutants also maintained normal MAPK activation when treated with RG-I oligomix or the 4+2 oligosaccharide (Fig. 5C and D). This suggests the existence of additional receptors with redundant functions, which were not tested in our initial screening or were not detected due to the sensitivity threshold of our screening system. To further investigate this possibility, we used MST to assess interactions between RG-I and three ARM1-proximal LRR-RKs in the ECD-based receptor similarity tree: two that were not included in our initial screening (AT5G43020 and AT3G50230) and one that was included (AT5G67200) (Fig. 5E and Supplementary Fig. 12A). MST analysis revealed that the interaction between AT5G43020^{ECD} and RG-I occurred with an EC50 value of 108.20 ± 22.68 μg/mL, which is slightly lower than that of ARM2b^{ECD}, while we were unable to obtain reliable interaction values for RG-I with ECDs of two other close homologs of ARM1, AT3G50230 and AT5G67200 (Fig. 5F). Thus, we designated AT5G43020 as ARM1c. These results suggest that functional redundancy in RG-I recognition may extend beyond the six ARMs we analyzed. We also observed that RG-I induced MAPK activation was not altered in well-studied co-receptor mutants in plant immunity such as *bak1* and *cerk1*, indicating that RG-I signaling is not mediated by BAK1 or CERK1 (Supplementary Fig. 12B and C).

Although the sextuple mutants showed similar immediate responses to RG-I treatment with regards to MAPK activation and defense-related gene induction, we found that the

sextuple mutants were more susceptible to infection by the foliar pathogen *Pseudomonas syringae pv. tomato* DC3000 compared to wild-type plants (Fig. 6). Collectively, these findings suggest that ARMs contribute to plant immunity through potentially complex and redundant mechanisms involving RG-I recognition.

Discussion

In land plants, pectin is a major component of the primary cell wall, accounting for approximately 30% of its dry weight[43]. Pectin consists of a group of highly complex and heterogeneous cell wall polysaccharides, organized into five major domains: homogalacturonan (HG), RG-I, RG-II, apiogalacturonan, and xylogalacturonan[44]. While the exact composition varies with environment, tissue type, and plant species, HG typically makes up around 60% of pectin and RG-I contributes 20% to 30%[45]. Although HG and RG-II are known to be involved in strengthening the cell wall, the specific function of RG-I remains less understood[44]. In this study, we identified new role of RG-I in plant defense responses, similar to that of OGs from HG or cellooligomers from cellulose, which function as DAMPs. RG-I specifically activates MAPK and induces defense genes without triggering Ca^{2+} influx or ROI production, unlike OGs and cellooligomers, which trigger all these responses (Fig. 3). These differences suggest that RG-I may play a specific role in plant immunity.

We identified that oligosaccharide fragments of RG-I can bind to ARM^{ECD}s and induce MAPK activation in Arabidopsis (Fig. 4). However, these oligosaccharides were less effective than RG-I polysaccharides. Given that longer OGs (DP 10-15) elicit stronger immune responses than shorter OGs, the RG-I fragments we tested could be less effective due to their shorter length. While both RG-I lyase and RG-I hydrolase produced RG-I oligosaccharides that activated MAPK similarly (Fig. 4C), further research is needed to understand which oligosaccharides are predominantly produced during biotic interactions in a natural context. Similarly to the profiling of OG fragments in Arabidopsis upon *Botrytis cinerea* infection[46], profiling RG-I fragments from interactions with microorganisms that contain RG-I lyases in their genomes, such as *Aspergillus niger* or *Bacillus subtilis*[47,48], need to be analyzed. Additionally, during the enzymatic digestion to fractionate RG-I oligosaccharides, we observed that in most oligosaccharides, at least one rhamnose residue is substituted with a single galactose. This suggests that galactose-substituted oligosaccharides might also be generated in a natural context, indicating potential functional significance. Chemically synthesizing these RG-I oligosaccharides will allow us to investigate their specific function[42].

The conventional approach to exploring novel ligand-receptor pairs involves first identifying the immunity-eliciting molecule and then finding its cognate receptor through forward genetics screening. However, this method faces significant limitations, particularly due to the functional redundancies of PRRs, except in rare cases where dominant negative mutations are generated. Our high-throughput screening pipeline was developed to overcome these limitations. Through the pipeline reported here, we identified five ARM receptors that interact with RG-I and its fragments, and additionally found that AT3G51740 (ARM2b) and AT5G43020 (ARM1c) showed reduced interaction activity with RG-I in MST analysis (Figs. 1D, 2B, and 5F). Although the *arm* sextuple mutants still exhibited MAPK activation upon RG-I treatment (Fig. 5), these mutants were less resistant to pathogen infection (Fig. 6), indicating that these receptors contribute to plant immunity. These observations are similar to those made for WAK receptors upon OGs perception. Recent findings suggest that additional receptors besides WAKs, including WAK-like (WAKL) family RKs, might be involved in OGs response based on analysis of *wak1-5* quintuple knock out mutants[16]. Similarly, we propose that additional redundant ARM receptors exist that were not tested in the screening due to either protein library limitations or insufficient affinity for glycan array detection. For example, ARM1c was not included in the initial screening but, when tested later, showed RG-I binding affinity (Fig. 5F). Therefore, we hypothesize that the maintained MAPK induction in the sextuple mutant might result from additional redundant ARM receptors that participate in Arabidopsis RG-I signaling. Furthermore, ARM receptors have distinct tissue-specific and developmental stage-specific expression patterns (Supplementary Fig. 13)[49,50]. These patterns may indicate a sophisticated regulatory system, potentially enabling ARM receptors to monitor cell wall dynamics in a spatially and temporally coordinated manner. Given that pectin dynamics are tightly regulated for cell wall integrity maintenance and cell morphogenesis[51], this diversity in expression likely enables robust surveillance of cell wall status across different tissues. This spatially coordinated expression of multiple receptors is reminiscent of the high-order regulation observed in the CLAVATA (CLV) signaling pathway, where BAM receptors exhibit tightly controlled spatial expression patterns regulated by CLV3-CLV1, leading to precise feedback control of stem cell populations[52]. Similarly, ARM receptor redundancy might reflect a system optimized for tissue-specific and context-dependent signaling, allowing plants to adapt to diverse physiological and environmental conditions. Together with the WAK-mediated OG recognition mechanisms, our findings uncover an additional layer of surveillance through ARM receptor-mediated RG-I recognition, which collectively establishes a sophisticated system for monitoring cell wall integrity via distinct pectin-derived DAMPs.

Our previous application of the high-throughput microarray approaches demonstrated their versatility in detecting ligand-receptor interactions by diversifying the ligand range for individual plant receptors[53,54]. Here, we expanded this approach by screening an extended plant receptor library against a collection of glycan molecules, including oligo- and polysaccharides. Our results validated this high-throughput screening pipeline for identifying novel ligand-receptor pairs. This versatile screening pipeline could be further expanded to explore crop plant receptor libraries and targeted glycan ligand libraries from specific structures of cell walls in fungi, oomycetes, or parasitic plants, paving the way for translational research.

Materials and Methods

Plant materials and growth conditions.

Arabidopsis thaliana accession Columbia (Col-0) was used as the wild-type and used for transgenic line generation. The mutant lines *cerk1* (SALK_007193), *bak1-4, bak1-5,* and *efr/fls2* were previously described[9,38,55]. The single T-DNA mutant lines *arm1a-2* (GABI_210H07), *arm1b-2* (GABI_510G08), *arm2a-1* (SALK_024031), *arm2a-2* (SAIL_600F09), *arm2b-2* (SALK_029864), *arm3a-1* (SALK_011390), *arm3a-2* (SALK_025297C), *arm3b-1* (SALK_071306), and *arm3b-2* (SALK_072419C) were genotyped using PCR and checked for full-length transcripts using RT-PCR, both with corresponding primers (Supplementary Table 4). Arabidopsis seeds were surface-sterilized and grown on Petri dishes containing ½ Murashige and Skoog (MS) medium with Gamborg B5 vitamins (Duchefa, M0231), 1% sucrose (Roth), and 0.8% agar (AppliChem), adjusted to pH 5.7 with KOH, in a growth room at 22 °C under long-day light conditions (16 h light/8 h dark). For the pMAPK, qPCR, or RNAseq experiments, 5-day-old Arabidopsis seedlings vertically grown on plates were transferred to a 6-well plate containing 2 mL of liquid media (½ MS including MES buffer (Duchefa, M0255) and 1% sucrose) and incubated further for 1 week. For the infection assays, Arabidopsis seeds were grown on soil in a growth chamber at 22 °C under day-neutral light conditions (12 h light/ 12 h dark).

Receptor similarity tree.

Protein sequences for receptors were obtained from a previous publication[56], while additional receptor proteins were obtained from TAIR (TAIR10_pep_20101214). A total of 518 candidate receptors were selected based on the functional domains identified by Pfam database [PMID: 39540428]. Transmembrane domains and transit peptides were analyzed using DeepTMHMM[57]. Then, receptor candidates without transmembrane domains or with an ECD length of less than 50 amino acids were excluded. The full protein sequences of 488 receptors were aligned with MAFFT[58]. Maximum likelihood trees were inferred with IQ-Tree, and support values for individual nodes were estimated using 1,000 pseudoreplicates of the ultrafast bootstrap approximation[59]. Trees with additional labels were visualized by iTOL v6[60].

S2 cell expression.

Recombinant ECDs of LRR-RK in pECIA2 expression vector, that provides a C-terminal Fc-tag, V5-tag and His-tag, were described previously[38], and additional ECDs were cloned into pECIA2 in this study. ECD expression was performed as previously described[61]. Briefly, expression clones were transiently transfected into *Drosophila* S2 cells (ExpreS2ion Biotechnologies) using the Expres2 TR transfection reagent (Expression Systems) and cultured at 27 °C. Upon transfection, the culturing temperature was switched to 25 °C. After 24 hours from transfection, protein expression was induced with 1 mM $CuSO_4$ for a further 72 hours. After expression, the supernatant including the secreted ECDs was collected and supplemented with cOmplete™, EDTA-free Protease Inhibitor (Roche, 11873580001) and 0.02% NaN_3. Protein expression was determined by immunoblotting using anti-V5-HRP antibodies (Invitrogen, R962-25).

Glycan array.

The plant glycan microarray was printed as previously described[39]. In brief, the synthetic oligosaccharides and commercially available polysaccharides were dissolved in the coupling buffer (150 mM sodium phosphate, pH 8.5) in a concentration of 200 µM for oligosaccharides and 200 µg/ml for polysaccharides (chitosan and 1,3-linked glucan at 20 µg/ml due to low solubility), and printed in triplicates on CodeLink N-hydroxyl succinimide (NHS) ester-activated glass slides (SurModics Inc., USA) using a non-contact piezoelectric spotting device (S3; Scienion, Germany). Sixteen identical fields as depicted in Supplementary Fig. 3 with all glycans in triplicates were printed on a glass slide. After printing, the remaining NHS groups on the microarray slides were quenched for 1 hour at RT using 100 mM ethanolamine, 50 mM sodium phosphate, pH 9. Then, the slides were washed three times with deionized water, dried and stored at 4 °C until usage. For the ECD binding assay, a 16-well grid was applied to the glass slide and the array was blocked for 45 min with 1 % bovine serum albumin (BSA) in binding buffer (20 mM HEPES, 100 mM NaCl, 1 mM $CaCl_2$, 1 mM $MnCl_2$, 1 mM $MgCl_2$, pH 6.8). Next, the supernatant of the insect cell media including the expressed ECDs was applied and incubated for 1 hour. After washing three times for 5 min with binding buffer, a polyclonal goat anti-human IgG antibody labeled with Alexa Fluor 647 (Invitrogen, A21445) diluted 1:400 in 1 % BSA in binding buffer was applied for 45 min. Then, the unbound secondary antibody was removed by washing once for 5 min with binding buffer including 0.1% Tween20, once 5 min with binding buffer, and rinsing the slide twice with water. The slides were scanned on a Genepix 4300A microarray scanner (Molecular Devices) using the 635 nm laser at photomultiplier gain PMT500. The images were obtained and analyzed using the GenePix Pro 7 software. For the enzymatic digest on the array, RG-I hydrolase (0.13 mg/ml in 100 mM sodium acetate buffer, pH 5.5), arabinofuranosidase or galactanase (10 U/ml in 100 mM sodium acetate buffer, pH4) were incubated in 100 µl reactions per well for 16 hours at 40°C. After washing twice with binding buffer, antibody staining using INRA-RU2 was performed as previously described[40] and the $ARM1a^{ECD}$ binding was conducted as described above.

Polysaccharides and oligosaccharides.

The sources of the purchased polysaccharides are indicated in Supplementary Table 2. The chemical synthesis of the oligosaccharides was previously described[62-68]. The branched RG-I oligosaccharides were prepared as follows: The side chains of the RG-I polysaccharide (5

mg/ml, Megazyme) were trimmed using arabinofuranosidase (AFASE, Megazyme, 5 U/ml) and galactanase (EGALN, Megazyme, 5 U/ml) in 100 mM sodium acetate buffer pH 4 at 40°C for 16 hours. After removing the arabinan and galactan fragments using dialysis (SnakeSkin dialysis tubes, 3.5 MWCO) for 8 hours at 4°C, exchanging the water three times, the resulting "RG-I trim" was digested using RG-I hydrolase (13 µg/ml) for 16 hours at 40°C in 100 mM sodium acetate pH 5. These "RG-I digest" still included hydrolytic enzymes that were heat-inactivated for 10 min at 85 °C. To obtain pure oligosaccharides, the sample was loaded on Carbograph solid phase extraction (SPE) columns (S*Pure) and was eluted using acetonitrile/0.25 % ammonium formiate buffer, pH 3 (1:1). Aliquots of the different samples in the purification process and the final "RG-I oligomix (Hydrolase oligomix)" were lyophilized. The same procedure was used to purify the "Lyase oligomix", except that RG-I lyase (18 µg/ml) was used. To analyze the composition of the RG-I hydrolase oligosaccharides a Shimadzu LC-MS system was used with a Hypercarb porous graphitized carbon (PGC) column (Thermo Fisher, 4.6x100 mm, 5 µm particle size) equipped with an Alltech 3000 Evaporative Light Scattering Detector (ELSD) and a Shimadzu LCMS-2020 mass spectrometer. To obtain defined individual oligosaccharides the RG-I oligosaccharide mixture was separated using HPLC with a semipreparative Hypercarb PGC column (Hypercarb, 10x100 mm, 7 µm particle size), The flow rate was 2 mL/min and the oligosaccharides were eluted applying a water (with 0.25 % ammonium formiate, pH 3), acetonitrile gradient starting with 5% acetonitrile (ACN) for 8 minutes followed by a ramp up to 30% ACN for 60 minutes, a short increase to 100% ACN for 4 minutes, a decline back to 5% and an equilibration at 5% ACN for 5 minutes. The fractions were collected in 30 seconds intervals and analyzed with LC-MS as described above and with MALDI-TOF-MS using the Autoflex Speed device (Bruker Daltonics, Germany) operated by the FlexControl 3.4 software. Fractions with the same oligosaccharide were pooled and the structures of the purified oligosaccharides were determined using nuclear magnetic resonance (NMR) analyses.

NMR analyses

Experiments were conducted on a Bruker III Avance 600 MHz spectrometer using Topspin 3.6.5 software. Spectra were recorded in D_2O at 300 K and referenced externally for ^1H to DSS in D_2O (0 ppm) and for ^{13}C to dioxane in D_2O (67.4 ppm). Standard pulse programs and settings from the Bruker library were employed unless otherwise stated. For recording HSQC spectra, a F1 FIDRes of 62 Hz (TD 1024) was achieved using non-uniform sampling with a NUS percentage of 40%. For HMBC, a F1 FIDRes of 65 Hz (TD 1024) was achieved using non-uniform sampling with a NUS percentage of 50%. Spectra were processed and assigned using Bruker Topspin 3.6.5.

ARM extracellular domain expression and purification.

ARM1a^{ECD} (residues 31-253), ARM1b^{ECD} (24-247), ARM2a^{ECD} (53-406), ARM2b^{ECD} (39-455), ARM3a^{ECD} (32-443), ARM3b^{ECD} (29-413), AT5G43020/ARM1c^{ECD} (29-248), AT3G50230^{ECD} (34-300), and AT5G67200^{ECD} (19-281) sequences were cloned into the pB1-Mel vector (Invitrogen) with a C-terminal StrepII-9×His tag, and used for Bacmid generation. After viral amplification, recombinant ECD proteins were expressed in *Trichoplusia ni* High Five insect cells (Expression Systems) at 21 °C for 72 hours. The secreted proteins were

purified using Ni-NTA affinity chromatography (HisTrap HP, Cytiva) with binding buffer (20 mM NaH_2PO_4/Na_2HPO_4 buffer pH 7.5, 500 mM NaCl, and 20 mM Imidazole) and subsequently size-exclusion chromatography (SEC) (Superdex 200 Increase 10/300 GL, Cytiva) with SEC buffer (20 mM NaH_2PO_4/Na_2HPO_4 buffer pH 7.5 and 200 mM NaCl).

MicroScale Thermophoresis (MST) assay.

The purified ECD proteins were labeled with the Monolith His-Tag Labeling Kit RED-tris-NTA 2nd Generation (MO-L018, NanoTemper) according to the manufacturer's instructions. 50 nM of labeled proteins and varying concentrations of ligands were mixed in MST buffer (20 mM NaH_2PO_4/Na_2HPO_4 buffer pH 7.5, 200 mM NaCl, 0.005% Tween-20), and then loaded into Monolith Premium Capillaries (MO-K025, NanoTemper). Measurements were performed at 25 °C in a Monolith NT.115 instrument with LED power set to 80% and MST power to 20% or 40%. Measurements were repeated at least three times. The data were analyzed by plotting the $\log_{10}$ values of ligand concentrations against the change in normalized thermophoresis (ΔFnorm [‰]) using MO.Affinity Analysis software (NanoTemper). The data were then analyzed with GraphPad Prism 10 software to fit curves and determine the EC50 or Kd values.

pMAPK assay.

Elicitor treatment was performed by replacing the previous media in the 6-well plates with new sterile MilliQ water containing each elicitor. 16 seedlings were used for total protein extraction. Total proteins were extracted in the extraction buffer (50 mM Tris-Cl pH 7.5, 150 mM NaCl, 2 mM Na_2MoO_4, 2 mM Na_3VO_4, 5 mM NaF, 2 mM phenylmethylsulfonyl fluoride, 1 mM DTT, 10% Glycerol, 1% IGEPAL, cOmplete™, EDTA-free Protease Inhibitor (Roche)). Immunodetection was performed using the anti-p44/p42 MAPK antibodies (9102, Cell Signaling; 1:5000) with anti-Rabbit-HRP antibodies (A6154, Sigma-Aldrich; 1:5000). Signals were detected with the ChemiDoc instrument (Bio-Rad).

Reactive oxygen intermediate (ROI) burst assay.

4 mm leaf discs from 6-week-old wild-type plants were placed in a 96-well luminescence assay plate, vacuum-infiltrated in sterile MilliQ water and incubated overnight. The water was replaced with a treatment solution containing elicitors, L-012 (Wako Chemicals), and horseradish peroxidase (Thermo Fisher Scientific). Relative luminescence was measured every minute for 120 min using a BiTec Synergy 4 microplate reader and summed for total photon counts.

Ca^{2+} influx measurement.

Col-0^{AEQ}, carrying the calcium reporter aequorin protein, were grown in a 96-well luminescence assay plate in liquid media (½ MS and 1% sucrose, adjusted pH 5.7) for 7 days. A day before the treatment, the media was replaced with 100 µL of 10 µM coelenterazine h (Biosynth, FC36332) solution and incubate for overnight in the darkness. Before treatment, the plates were scanned for 1 min (300 msec per well with 6 sec interval) to obtain resting level readings using a Spark Cyto microplate reader (TECAN). For treatment, 50 µL of 3-fold concentrated elicitor solutions were added to the plates, and further scans were conducted for 25 min.

RNAseq analysis

12-day-old Arabidopsis seedlings grown in 6-well plates were treated for 0min, 30 min, or 90 min with 100 µg/mL of RG-I polysaccharide. Total RNA was isolated from pools of 16 seedlings using the RNeasy Plant Mini Kit (QIAGEN). All samples were prepared in triple replication from independent experiments. Five hundred nanograms of total RNA from each sample was used for cDNA and NGS library preparations with the QuantSeq 3' mRNA-Seq Library Prep kit (FWD) (Lexogen, 015). The individual NGS libraries were pooled in equimolar ratios and sequenced on a NovaseqS4 in single end-150 base mode. The quality check of raw reads was conducted by FastQC (ver 0.11.9). The reads were processed and quantified against the reference transcriptome (TAIR10.transcripts.fa) using Kallisto (ver 0.46.2). The Kallisto-processed reads from OGs treatment were retrieved from a previous study () using getDEE2 (ver 1.14.0). The abundance results were analyzed using DESeq2 (ver 1.44.0). Differentially expressed genes (DEGs) were identified with a cut-off of |Log2FC| > 1 and Padj < 0.05. These DEGs were then used to generate a heatmap with the pheatmap package (ver 1.0.12) and a Venn diagram with the ggvenn package (ver 0.1.10). Gene Ontology (GO) analysis was performed using the enrichGO function from the clusterProfiler package (ver 4.12.2) to assess biological processes (BP). Enriched functions were emphasized with a bubble-chart, excluding the hypoxia-related gene sets considered as artifacts of the treatment method to avoid misinterpretation. The RNA-seq datasets generated and analyzed in the current study have been deposited in the Sequence Read Archive at NCBI under bioproject accession code PRJNA1195916.

RT-qPCR analysis.

Elicitor solution treatment was performed by replacing the previous media in the 6-well plates with new sterile MilliQ water containing each elicitor. After replacement, the plates were vacuum infiltrated for 10 min and incubated 1 hour or 2 hours. 8 or 16 seedlings were used for total RNA extraction. Total RNA was isolated using the GeneMATRIX Universal RNA Purification Kit (EURx). Subsequently, one microgram of isolated total RNA was used for cDNA synthesis with the RevertAid First Strand cDNA Synthesis Kit (Thermo Fisher Scientific). qPCR analyses were performed with Takyon ROX SYBR 2X MasterMix dTTP blue (Eurogentec, UF-RSMT-B0701) with target primers (Supplementary Table 4) using a Bio-Rad CFX Opus Real-Time PCR system. Actin2/8 cycle threshold (Ct) was used as an endogenous control and ΔCt of mock treatment for each genotype was used for normalization.

CRISPR/Cas9 genome editing.

CRISPR/Cas9 genome editing was performed as previously described[69]. Briefly, the selected guide RNA (gRNA) sequences targeting the ARM genes were inserted into the guide RNA scaffold (sgRNA) GreenGate entry vectors. The annealed reverse and forward complement sequences of the gRNA primers, each with different overhangs (Supplementary Table 4), were ligated into the entry vector cut with BpiI (New England Biolabs, FD1014). ARM1a sgRNA1 and ARM1b sgRNA2 entry clones were assembled into the destination vector pGGZ003 using the GreenGate reaction, together with entry clones containing the *Petroselinum crispum* ubiquitin4-2 promoter, codon-optimized Cas9, *Pisum sativum* pea3A terminator, and seedcoat-

localized YFP (pAlligator:YFP). The same process was applied to ARM2a sgRNA1 and ARM2b sgRNA2, as well as to ARM3a sgRNA1 and ARM3b sgRNA2. Each destination vector was introduced into *Agrobacterium tumefaciens* (GV3101 pSoup). Wild-type Arabidopsis was then transformed with these destination vectors to generate single or double mutants using the floral dip method. YFP-positive T1 seeds were grown on soil, and PCR was performed using the corresponding primer sets (Supplementary Table 4). The PCR products were sequenced with the Sanger method and analyzed with the Tide program (http://shinyapps.datacurators.nl/tide/). YFP-negative T2 seeds were selected to obtain plants lacking the Cas9 cassette and analyzed by sequencing using the same methods. Higher-order mutants, such as quadruple or sextuple mutants, were generated by introducing additional gRNA sets into the double mutants or quadruple mutant, respectively.

Bacterial infection assays

4-week-old Arabidopsis plants grown on soil were sprayed with a *Pseudomonas syringae pv. tomato* DC3000 inoculum at OD_{600} = 0.2 in 10 mM $MgCl_2$ supplemented with 0.02% Silwet L-77. Three days after inoculation, 8 leaf discs from 4 independent plants were bored, ground, and homogenized in 10 mM $MgCl_2$. The bacterial titer was assessed by serial dilution plating. Representative picture was acquired five days after inoculation. The disease index was calculated by dividing the number of infected leaves (more than half of the leaf being yellow) by total number of leaves.

Data visualization and statistical analysis

GraphPad PRISM 10 and R (version 4.4.1 with Bioconductor) were used for data analysis and visualization. Statistical analyses were performed using either one-way ANOVA (two-sided) followed by Tukey's multiple comparisons test in GraphPad PRISM, or linear mixed-effects modeling followed by one-way ANOVA (two-sided) with Tukey's multiple comparisons test in R. For linear mixed-effects modeling, we used the lme4 package (version 1.1-35.5), with wild-type control or mock treatment as fixed effects and experimental replicates as random effects, using the formula: Value ~ treatment + (1|Trial). Values were $\log_{10}$-transformed when this improved the fit to the linear model. Different letters above the plot indicate significant differences between groups based on all pairwise comparisons using multiple comparisons tests.

Code availability

All source codes that we used in this study are also available in *Zenodo*.
[https://doi.org/10.5281/zenodo.14760738]

Acknowledgements

We thank Dr. Antonio Molina at the technical university of Madrid for providing Col-0^{AEQ} transgenic line seeds and Dr. Cecilia Romanò and Dr. Mads Clausen at the Technical University of Denmark for providing the synthetic RG-I heptasaccharide. The RG-I hydrolase and RG-I lyase were a kind gift from Dr. Kristian Bertel Krogh at Novozymes, Denmark. We thank Julia Watzal and Julian Bünting for technical assistance. Finally, we thank Jana Neuhold, Orla Dunne, and Aranxa Caballero at the Vienna Biocenter Core Facilities (VBCF Protech) for help in molecular cloning and protein production, the VBCF Plant Sciences facilities for the plant

growth chambers, and NGS facility. This work was funded in part by the Austrian Science Fund (FWF) by a grant to F. P. [P 35404]. This work was also supported by grants from the Austrian Academy of Science through the Gregor Mendel Institute, the Vienna Science and Technology Fund Project to Y.B. [LS17-047], and by a grant from the National Research Foundation of Korea to H.S.L. [RS-2024–00338015]. This project was supported by the BOKU Core Facility Mass Spectrometry.

Author contributions

Project Administration, Y.B. and F.P.; Conceptualization, D.H.L., C.R., Y.B., and F.P.; Investigation, D.H.L, C.R., J.M.L, M.S.C, T.H., G.H., N.E., B.E., and M.B.; Supervision, D.H.L., C.R., Y.B., and F.P.; Methodology, D.H.L., C.R., J.M.L, M.S.C, T.H., G.H., N.E., B.E., M.B., C.H.C., H.S.L., and Y.B.; Resources, D.H.L., C.R., Y.B., E.S.L., and F.P.,; Software, D.H.L., C.R., and F.P.; Formal Analysis, D.H.L. and C.R.; Validation, D.H.L., C.R., and F.P.; Writing-Original Draft, D.H.L., C.R., and F.P.; Writing-Review & Editing, all other authors commented and agreed on the manuscript; Visualization, D.H.L. and C.R.

Author Information

The authors declare no competing interests.

References

1 Wolf, S. Cell Wall Signaling in Plant Development and Defense. *Annu Rev Plant Biol* **73**, 323-353 (2022). https://doi.org/10.1146/annurev-arplant-102820-095312

2 Delmer, D., Dixon, R. A., Keegstra, K. & Mohnen, D. The plant cell wall-dynamic, strong, and adaptable-is a natural shapeshifter. *Plant Cell* **36**, 1257-1311 (2024). https://doi.org/10.1093/plcell/koad325

3 Malinovsky, F. G., Fangel, J. U. & Willats, W. G. The role of the cell wall in plant immunity. *Front Plant Sci* **5**, 178 (2014). https://doi.org/10.3389/fpls.2014.00178

4 Molina, A. *et al.* Plant cell wall-mediated disease resistance: Current understanding and future perspectives. *Mol Plant* **17**, 699-724 (2024). https://doi.org/10.1016/j.molp.2024.04.003

5 Bacete, L., Mélida, H., Miedes, E. & Molina, A. Plant cell wall-mediated immunity: cell wall changes trigger disease resistance responses. *The Plant Journal* **93**, 614-636 (2018). https://doi.org/10.1111/tpj.13807

6 Lee, D.-H., Lee, H.-S. & Belkhadir, Y. Coding of plant immune signals by surface receptors. *Current Opinion in Plant Biology* **62**, 102044 (2021). https://doi.org/10.1016/j.pbi.2021.102044

7 DeFalco, T. A. & Zipfel, C. Molecular mechanisms of early plant pattern-triggered immune signaling. *Molecular Cell* **81**, 3449-3467 (2021). https://doi.org/10.1016/j.molcel.2021.07.029

8 Cao, Y. *et al.* The kinase LYK5 is a major chitin receptor in Arabidopsis and forms a chitin-induced complex with related kinase CERK1. *eLife* **3**, e03766 (2014). https://doi.org/10.7554/elife.03766

9 Miya, A. *et al.* CERK1, a LysM receptor kinase, is essential for chitin elicitor signaling in Arabidopsis. *Proceedings of the National Academy of Sciences* **104**, 19613-19618 (2007). https://doi.org/10.1073/pnas.0705147104

10 Kaku, H. *et al.* Plant cells recognize chitin fragments for defense signaling through a plasma membrane receptor. *Proceedings of the National Academy of Sciences* **103**, 11086-11091 (2006). https://doi.org/10.1073/pnas.0508882103
11 Brutus, A., Sicilia, F., Macone, A., Cervone, F. & Lorenzo, G. D. A domain swap approach reveals a role of the plant wall-associated kinase 1 (WAK1) as a receptor of oligogalacturonides. *Proceedings of the National Academy of Sciences* **107**, 9452-9457 (2010). https://doi.org/10.1073/pnas.1000675107
12 Hématy, K., Cherk, C. & Somerville, S. Host-pathogen warfare at the plant cell wall. *Curr Opin Plant Biol* **12**, 406-413 (2009). https://doi.org/10.1016/j.pbi.2009.06.007
13 Xiao, Y. *et al.* A plant mechanism of hijacking pathogen virulence factors to trigger innate immunity. *Science* **383**, 732-739 (2024). https://doi.org/10.1126/science.adj9529
14 Côté, F. & Hahn, M. G. Oligosaccharins: structures and signal transduction. *Plant Mol Biol* **26**, 1379-1411 (1994). https://doi.org/10.1007/BF00016481
15 Denoux, C. *et al.* Activation of defense response pathways by OGs and Flg22 elicitors in Arabidopsis seedlings. *Mol Plant* **1**, 423-445 (2008). https://doi.org/10.1093/mp/ssn019
16 Herold, L. *et al.* Arabidopsis WALL-ASSOCIATED KINASES are not required for oligogalacturonide-induced signaling and immunity. *bioRxiv* (2024). https://doi.org/10.1101/2024.04.15.589471
17 Kohorn, B. D., Greed, B. E., Mouille, G., Verger, S. & Kohorn, S. L. Effects of Arabidopsis wall associated kinase mutations on ESMERALDA1 and elicitor induced ROS. *PLoS One* **16**, e0251922 (2021). https://doi.org/10.1371/journal.pone.0251922
18 Martín-Dacal, M. *et al.* Arabidopsis immune responses triggered by cellulose and mixed-linked glucan oligosaccharides require a group of Leucine-Rich Repeat-Malectin Receptor Kinases. *The Plant Journal* (2022). https://doi.org/10.1111/tpj.16088
19 Tseng, Y. H. *et al.* CORK1, A LRR-Malectin Receptor Kinase, Is Required for Cellooligomer-Induced Responses in. *Cells* **11** (2022). https://doi.org/10.3390/cells11192960
20 Kubicek, C. P., Starr, T. L. & Glass, N. L. Plant cell wall-degrading enzymes and their secretion in plant-pathogenic fungi. *Annu Rev Phytopathol* **52**, 427-451 (2014). https://doi.org/10.1146/annurev-phyto-102313-045831
21 Bacete, L. *et al.* Plant Pattern Recognition Receptors, Methods and Protocols. *Methods in Molecular Biology* **1578**, 13-23 (2017). https://doi.org/10.1007/978-1-4939-6859-6_2
22 Aziz, A. *et al.* Elicitor and resistance-inducing activities of β-1,4 cellodextrins in grapevine, comparison with β-1,3 glucans and α-1,4 oligogalacturonides. *Journal of Experimental Botany* **58** (2007). https://doi.org/10.1093/jxb/erm008
23 Claverie, J. *et al.* The Cell Wall-Derived Xyloglucan Is a New DAMP Triggering Plant Immunity in Vitis vinifera and Arabidopsis thaliana. *Frontiers in Plant Science* **9**, 1725 (2018). https://doi.org/10.3389/fpls.2018.01725
24 Klarzynski, O. *et al.* Linear β-1,3 Glucans Are Elicitors of Defense Responses in Tobacco. *Plant Physiology* **124** (2000). https://doi.org/10.1104/pp.124.3.1027
25 Mélida, H. *et al.* Non-branched β-1,3-glucan oligosaccharides trigger immune responses in Arabidopsis. *The Plant Journal* **93**, 34-49 (2018). https://doi.org/10.1111/tpj.13755
26 Mélida, H. *et al.* Arabinoxylan-Oligosaccharides Act as Damage Associated Molecular Patterns in Plants Regulating Disease Resistance. *Frontiers in Plant Science* **11**, 1210 (2020). https://doi.org/10.3389/fpls.2020.01210

27 Wanke, A. *et al.* Plant species-specific recognition of long and short β-1,3-linked glucans is mediated by different receptor systems. *The Plant Journal* **102**, 1142-1156 (2020). https://doi.org/10.1111/tpj.14688
28 Bjornson, M., Pimprikar, P., Nürnberger, T. & Zipfel, C. The transcriptional landscape of Arabidopsis thaliana pattern-triggered immunity. *Nature Plants* **7**, 579-586 (2021). https://doi.org/10.1038/s41477-021-00874-5
29 Bigeard, J., Colcombet, J. & Hirt, H. Signaling mechanisms in pattern-triggered immunity (PTI). *Mol Plant* **8**, 521-539 (2015). https://doi.org/10.1016/j.molp.2014.12.022
30 He, Z., Webster, S. & He, S. Y. Growth-defense trade-offs in plants. *Curr Biol* **32**, R634-R639 (2022). https://doi.org/10.1016/j.cub.2022.04.070
31 Gómez-Gómez, L., Felix, G. & Boller, T. A single locus determines sensitivity to bacterial flagellin in Arabidopsis thaliana. *Plant J* **18**, 277-284 (1999). https://doi.org/10.1046/j.1365-313x.1999.00451.x
32 Jing, Y. *et al.* Danger-Associated Peptides Interact with PIN-Dependent Local Auxin Distribution to Inhibit Root Growth in Arabidopsis. *Plant Cell* **31**, 1767-1787 (2019). https://doi.org/10.1105/tpc.18.00757
33 Choi, J. *et al.* Identification of a Plant Receptor for Extracellular ATP. *Science* **343**, 290-294 (2014). https://doi.org/10.1126/science.343.6168.290
34 Ranf, S. *et al.* A lectin S-domain receptor kinase mediates lipopolysaccharide sensing in Arabidopsis thaliana. *Nature Immunology* **16**, 426-433 (2015). https://doi.org/10.1038/ni.3124
35 Yamaguchi, Y., Huffaker, A., Bryan, A. C., Tax, F. E. & Ryan, C. A. PEPR2 is a second receptor for the Pep1 and Pep2 peptides and contributes to defense responses in Arabidopsis. *Plant Cell* **22**, 508-522 (2010). https://doi.org/10.1105/tpc.109.068874
36 Liu, C., Yu, H., Voxeur, A., Rao, X. & Dixon, R. A. FERONIA and wall-associated kinases coordinate defense induced by lignin modification in plant cell walls. *Sci Adv* **9**, eadf7714 (2023). https://doi.org/10.1126/sciadv.adf7714
37 Wang, L. *et al.* The systemin receptor SYR1 enhances resistance of tomato against herbivorous insects. *Nature Plants* **4**, 152-156 (2018). https://doi.org/10.1038/s41477-018-0106-0
38 Smakowska-Luzan, E. *et al.* An extracellular network of Arabidopsis leucine-rich repeat receptor kinases. *Nature* **553**, 342-346 (2018). https://doi.org/10.1038/nature25184
39 Ruprecht, C. *et al.* A Glycan Array-Based Assay for the Identification and Characterization of Plant Glycosyltransferases. *Angewandte Chemie International Edition* **59**, 12493-12498 (2020). https://doi.org/10.1002/anie.202003105
40 Ruprecht, C. *et al.* A Synthetic Glycan Microarray Enables Epitope Mapping of Plant Cell Wall Glycan-Directed Antibodies. *Plant Physiology* **175**, 1094-1104 (2017). https://doi.org/10.1104/pp.17.00737
41 MC, R., O, T., D, P., A, M. & F, G. Monoclonal antibodies to rhamnogalacturonan I backbone - PubMed. *Planta* **231** (2010). https://doi.org/10.1007/s00425-010-1116-y
42 Romanò, C., Awan, S. & Clausen, M. H. Chemical synthesis of branched rhamnogalacturonan I oligosaccharides. (2024). https://doi.org/10.26434/chemrxiv-2024-nlf7p
43 Willats, W. G., McCartney, L., Mackie, W. & Knox, J. P. Pectin: cell biology and prospects for functional analysis. *Plant Mol Biol* **47**, 9-27 (2001).
44 Harholt, J., Suttangkakul, A. & Vibe Scheller, H. Biosynthesis of pectin. *Plant Physiol* **153**, 384-395 (2010). https://doi.org/10.1104/pp.110.156588

45 Mohnen, D. Pectin structure and biosynthesis. *Curr Opin Plant Biol* **11**, 266-277 (2008). https://doi.org/10.1016/j.pbi.2008.03.006
46 Voxeur, A. *et al.* Oligogalacturonide production upon Arabidopsis thaliana–Botrytis cinerea interaction. *Proceedings of the National Academy of Sciences* **116**, 19743-19752 (2019). https://doi.org/10.1073/pnas.1900317116
47 Ochiai, A., Itoh, T., Kawamata, A., Hashimoto, W. & Murata, K. Plant Cell Wall Degradation by Saprophytic Bacillus subtilis Strains: Gene Clusters Responsible for Rhamnogalacturonan Depolymerization. *Applied and Environmental Microbiology* **73**, 3803-3813 (2007). https://doi.org/10.1128/aem.00147-07
48 Khosravi, C. *et al.* In vivo functional analysis of L-rhamnose metabolic pathway in Aspergillus niger: a tool to identify the potential inducer of RhaR. *BMC Microbiology 2017 17:1* **17** (2017). https://doi.org/10.1186/s12866-017-1118-z
49 Mergner, J. *et al.* Mass-spectrometry-based draft of the Arabidopsis proteome. *Nature* **579**, 409-414 (2020). https://doi.org/10.1038/s41586-020-2094-2
50 Wu, Y. *et al.* Genome-Wide Expression Pattern Analyses of the Arabidopsis Leucine-Rich Repeat Receptor-Like Kinases. *Molecular Plant* **9**, 289-300 (2016). https://doi.org/10.1016/j.molp.2015.12.011
51 Du, J., Anderson, C. T. & Xiao, C. Dynamics of pectic homogalacturonan in cellular morphogenesis and adhesion, wall integrity sensing and plant development. *Nature Plants* **8**, 332-340 (2022). https://doi.org/10.1038/s41477-022-01120-2
52 Nimchuk, Z. L., Zhou, Y., Tarr, P. T., Peterson, B. A. & Meyerowitz, E. M. Plant stem cell maintenance by transcriptional cross-regulation of related receptor kinases. *Development* **142**, 1043-1049 (2015). https://doi.org/10.1242/dev.119677
53 Parys, K. *et al.* Signatures of antagonistic pleiotropy in a bacterial flagellin epitope. *Cell Host & Microbe* **29**, 620-634.e629 (2021). https://doi.org/10.1016/j.chom.2021.02.008
54 Lee, D.-H. *et al.* Reprogramming of flagellin receptor responses with surrogate ligands. *Nature Communications* **15** (2024). https://doi.org/10.1038/s41467-024-54271-5
55 Schwessinger, B. *et al.* Phosphorylation-Dependent Differential Regulation of Plant Growth, Cell Death, and Innate Immunity by the Regulatory Receptor-Like Kinase BAK1. *PLoS Genetics* **7**, e1002046 (2011). https://doi.org/10.1371/journal.pgen.1002046
56 Ngou, B. P. M., Heal, R., Wyler, M., Schmid, M. W. & Jones, J. D. G. Concerted expansion and contraction of immune receptor gene repertoires in plant genomes. *Nature Plants* **8**, 1146-1152 (2022). https://doi.org/10.1038/s41477-022-01260-5
57 Hallgren, J. *et al.* DeepTMHMM predicts alpha and beta transmembrane proteins using deep neural networks. *bioRxiv* (2022). https://doi.org/10.1101/2022.04.08.487609
58 Rozewicki, J., Li, S., Amada, K. M., Standley, D. M. & Katoh, K. MAFFT-DASH: integrated protein sequence and structural alignment. *Nucleic Acids Res* **47**, W5-W10 (2019). https://doi.org/10.1093/nar/gkz342
59 Minh, B. Q. *et al.* IQ-TREE 2: New Models and Efficient Methods for Phylogenetic Inference in the Genomic Era. *Mol Biol Evol* **37**, 1530-1534 (2020). https://doi.org/10.1093/molbev/msaa015
60 Letunic, I. & Bork, P. Interactive Tree of Life (iTOL) v6: recent updates to the phylogenetic tree display and annotation tool. *Nucleic Acids Res* **52**, W78-W82 (2024). https://doi.org/10.1093/nar/gkae268
61 Clasen, S. J. *et al.* Silent recognition of flagellins from human gut commensal bacteria by Toll-like receptor 5. *Science immunology* **8**, eabq7001 (2023). https://doi.org/10.1126/sciimmunol.abq7001

62 Bartetzko, M. P., Schuhmacher, F., Seeberger, P. H. & Pfrengle, F. Determining Substrate Specificities of β1,4-Endogalactanases Using Plant Arabinogalactan Oligosaccharides Synthesized by Automated Glycan Assembly. *J Org Chem* **82**, 1842-1850 (2017). https://doi.org/10.1021/acs.joc.6b02745

63 Dallabernardina, P., Schuhmacher, F., Seeberger, P. H. & Pfrengle, F. Automated glycan assembly of xyloglucan oligosaccharides. *Org Biomol Chem* **14**, 309-313 (2016). https://doi.org/10.1039/c5ob02226f

64 Dallabernardina, P., Schuhmacher, F., Seeberger, P. H. & Pfrengle, F. Mixed-Linkage Glucan Oligosaccharides Produced by Automated Glycan Assembly Serve as Tools To Determine the Substrate Specificity of Lichenase. *Chemistry* **23**, 3191-3196 (2017). https://doi.org/10.1002/chem.201605479

65 Schmidt, D., Schuhmacher, F., Geissner, A., Seeberger, P. H. & Pfrengle, F. Automated synthesis of arabinoxylan-oligosaccharides enables characterization of antibodies that recognize plant cell wall glycans. *Chemistry* **21**, 5709-5713 (2015). https://doi.org/10.1002/chem.201500065

66 Senf, D. *et al.* Active Site Mapping of Xylan-Deconstructing Enzymes with Arabinoxylan Oligosaccharides Produced by Automated Glycan Assembly. *Chemistry* **23**, 3197-3205 (2017). https://doi.org/10.1002/chem.201605902

67 Bartetzko, M. P., Schuhmacher, F., Hahm, H. S., Seeberger, P. H. & Pfrengle, F. Automated Glycan Assembly of Oligosaccharides Related to Arabinogalactan Proteins. *Org Lett* **17**, 4344-4347 (2015). https://doi.org/10.1021/acs.orglett.5b02185

68 Zakharova, A. N., Madsen, R. & Clausen, M. H. Synthesis of a backbone hexasaccharide fragment of the pectic polysaccharide rhamnogalacturonan I. *Org Lett* **15**, 1826-1829 (2013). https://doi.org/10.1021/ol400430p

69 Richter, J. *et al.* Multiplex mutagenesis of four clustered CrRLK1L with CRISPR/Cas9 exposes their growth regulatory roles in response to metal ions. *Sci Rep* **8**, 12182 (2018). https://doi.org/10.1038/s41598-018-30711-3

70 Eby, R. & Schuerch, C. Synthesis and characterization of methyl 2-O-β-d-galactopyranosyl-β-d-galactopyranoside and methyl 2-O-(2-O-β-d-galactopyranosyl-β-d-galactopyranosyl)-β-d-galactopyranoside. *Carbohydrate Research* **92** (1981). https://doi.org/10.1016/S0008-6215(00)85990-X

71 Bock, K. & Thøgersen, H. in *Annual Reports on NMR Spectroscopy* Vol. 13 (ed G. A. Webb) 1-57 (Academic Press, 1983).

72 Waese, J. *et al.* ePlant: Visualizing and Exploring Multiple Levels of Data for Hypothesis Generation in Plant Biology. *The Plant Cell* **29**, 1806-1821 (2017). https://doi.org/10.1105/tpc.17.00073

Figure legends

Fig. 1

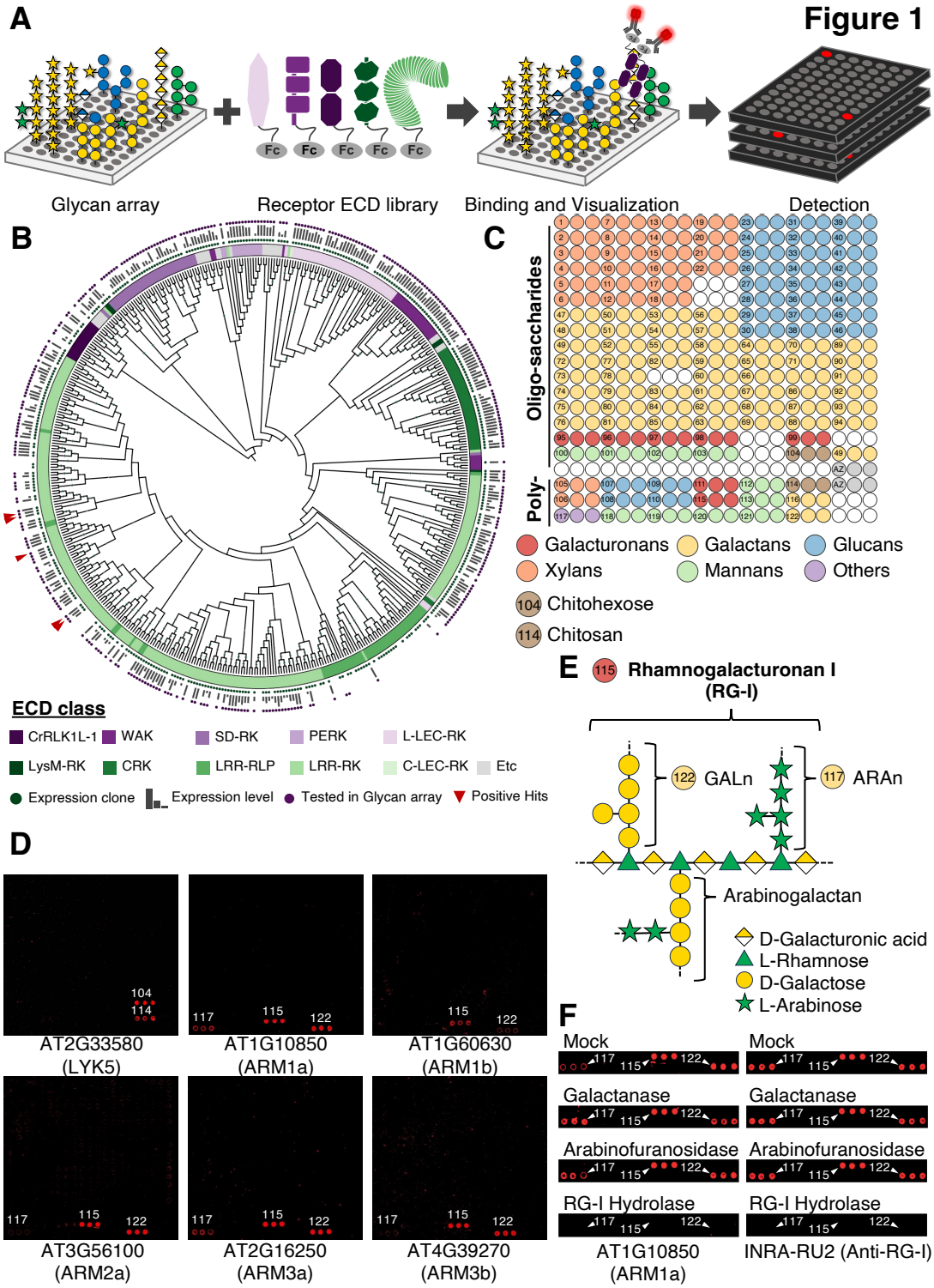

Fig. 1. High-throughput plant glycan array screening revealed that five ECDs of LRR-RKs interact with polysaccharides related to Rhamnogalacturonan-I (RG-I).

A. A schematic representation of the screening pipeline using a recombinant ECD library of Arabidopsis receptors and a plant glycan array. **B.** A receptor similarity tree based on ECD sequence similarity of all Arabidopsis plasma membrane-located receptor proteins. ECD

classes were distinguished by different color codes. Bootstrap values above 50 are represented with different dot sizes on each node. Detailed information is available in Supplementary Fig. 1. **C.** Printing pattern for the plant glycan array. Detailed information is available in Supplementary Fig. 3. **D.** Positive hits from screening results. The chitin receptor LYK5 (AT2G33580) was used as a positive control. Numbers indicate the printed regions that described in (C). **E.** Structure of RG-I showing the overlapped interaction across five ECDs of LRR-RKs. **F.** On-array digestion was performed with either galactanase, arabinofuranosidase, or RG-I hydrolase. $ARM1^{ECD}$ was used for determination of binding on the glycan array after digestion. RG-I-specific antibodies, INRA-RU2 (anti-RG-I backbone) was used for checking the clear digestion. Numbers indicate the printed regions that described in (C).

Fig. 2

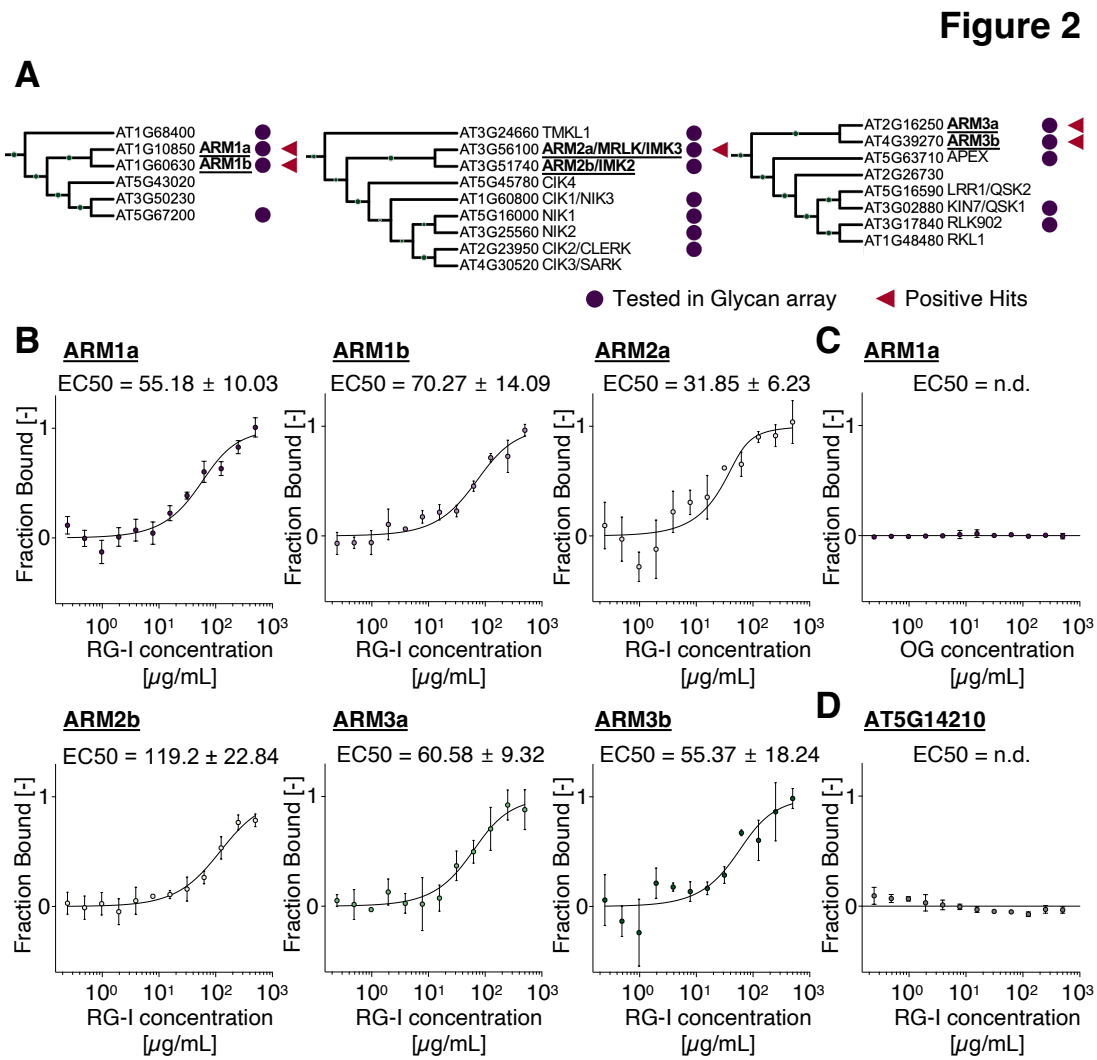

Fig. 2. Quantification of binding between RG-I and ARM^{ECD}s using Microscale thermophoresis (MST).

A. ARM-containing clades from the receptor similarity tree based on ECD sequences. **B.** Quantification of interaction between RG-I and ARM^{ECD}s using MST. Data points in the fitted-dose response binding curve indicate the fraction of labeled ARM^{ECD} bound to RG-I (mean ± SE; n=4). **C.** MST result for the interaction of OGs (OG$^{DP10-15}$) with ARM1^{ECD} (mean ± SE; n=3). **D.** MST result for the interaction between RG-I and AT5G14210^{ECD} (mean ± SE; n=3).

Fig. 3

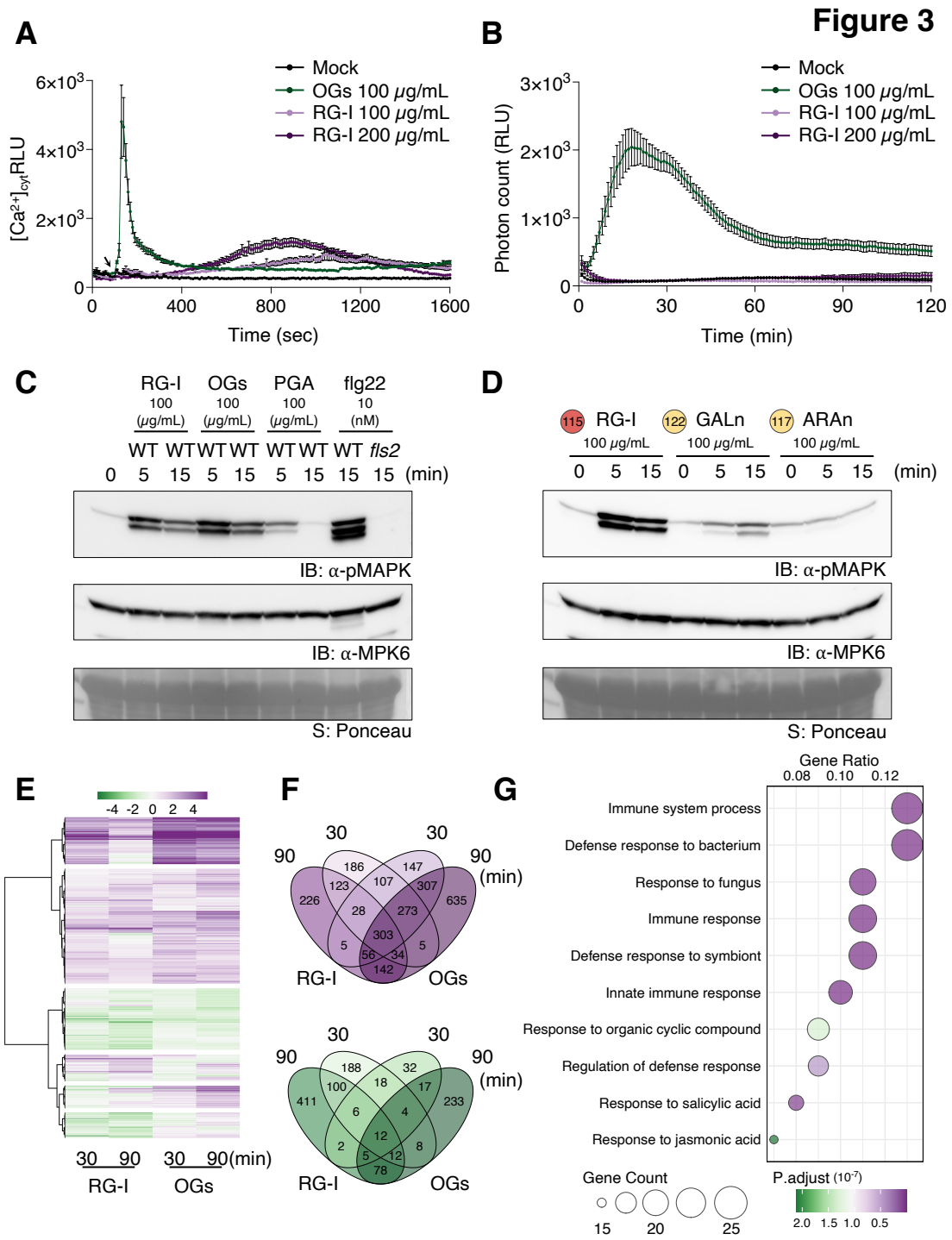

Fig. 3. RG-I treatment induces canonical immune response outputs except for acute accumulation of cytosolic Ca^{2+} and ROI production.

A. Cytosolic Ca^{2+} ion influx patterns were measured using the WT^{AEQ} reporter line upon treatment with either Mock, OGs ($OG^{DP10-15}$), or RG-I (mean ± SE; n=20). The arrow indicates the treatment points (60 sec). **B.** Reactive oxygen intermediates (ROI) production kinetics after treatment with Mock, OGs, or RG-I (mean ± SE; n=24). **C and D.** Immunoblotting (IB) analysis of MAPK phosphorylation in wild-type (WT) or *fls2* mutant Arabidopsis seedlings treated with OGs, polygalacturonic acid (PGA), RG-I, or flg22 (C). IB analysis of MAPK

phosphorylation in wild-type (WT) Arabidopsis seedlings treated with RG-I, Galactan (GALn) or Arabinan (ARAn) (D). Treatments, concentrations, and durations are shown on top. This experiment was repeated twice with similar results. Equal loading of protein samples on the blot was controlled by anti-MPK6 blotting (middle) and by Ponceau stain (bottom) visualizing Rubisco large subunit (rbcL). **E.** Heatmap of differentially expressed genes (DEGs) in WT seedlings treated for 30 min or 90 min with 100 µg/mL of RG-I or OGs. DEGs of OGs were retrieved from a previous study[28]. **F.** Venn diagrams showing the overlap of RG-I (left) and OGs (right) DEGs. Upregulated and downregulated DEGs are shown at the top and bottom, respectively. DEG numbers are indicated in the circles. **G.** Gene Ontology (GO) analysis showing enrichment in biological process categories from overlapped 303 upregulated DEGs at both 30 min and 90 min following RG-I and OGs treatment. Bubble chart indicates the calculated gene ratio in each GO term with adjusted P-values.

Fig. 4

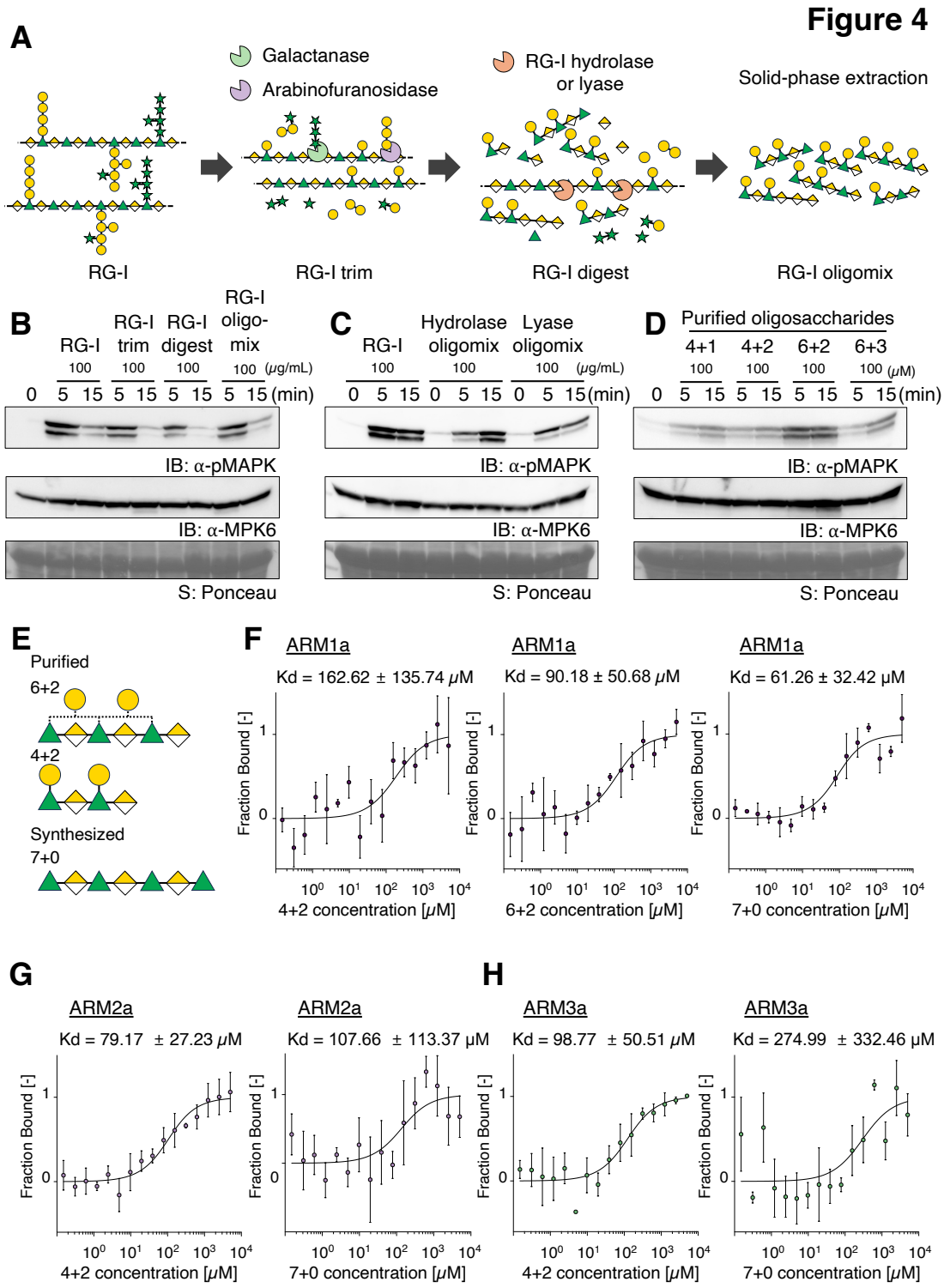

Fig. 4. Specific RG-I derived oligosaccharides induce MAPK activation and interact with ARM^{ECD}s.

A. Schematic representation of the enzymatic digestion and preparation of RG-I fragments. **B-D.** Immunoblotting (IB) analyses of MAPK phosphorylation in wild-type (WT) Arabidopsis seedlings treated with either RG-I or RG-I fragments. Treatment conditions, including concentrations and durations, are indicated at the top of the blots. This experiment was repeated

twice with similar results. Equal loading of protein samples on the blot was controlled by anti-MPK blotting (middle) and Ponceau staining (bottom), which visualizes the Rubisco large subunit (rbcL). **E.** Structures of oligosaccharides used in MST assay. **F-H**. Quantification of interaction between RG-I oligosaccharides and ARM^{ECD}s using MST. Data points in the fitted-dose response binding curves indicate the fraction of labeled ARM^{ECD} bound to each oligosaccharide as described (mean ± SE; n=4).

Fig. 5

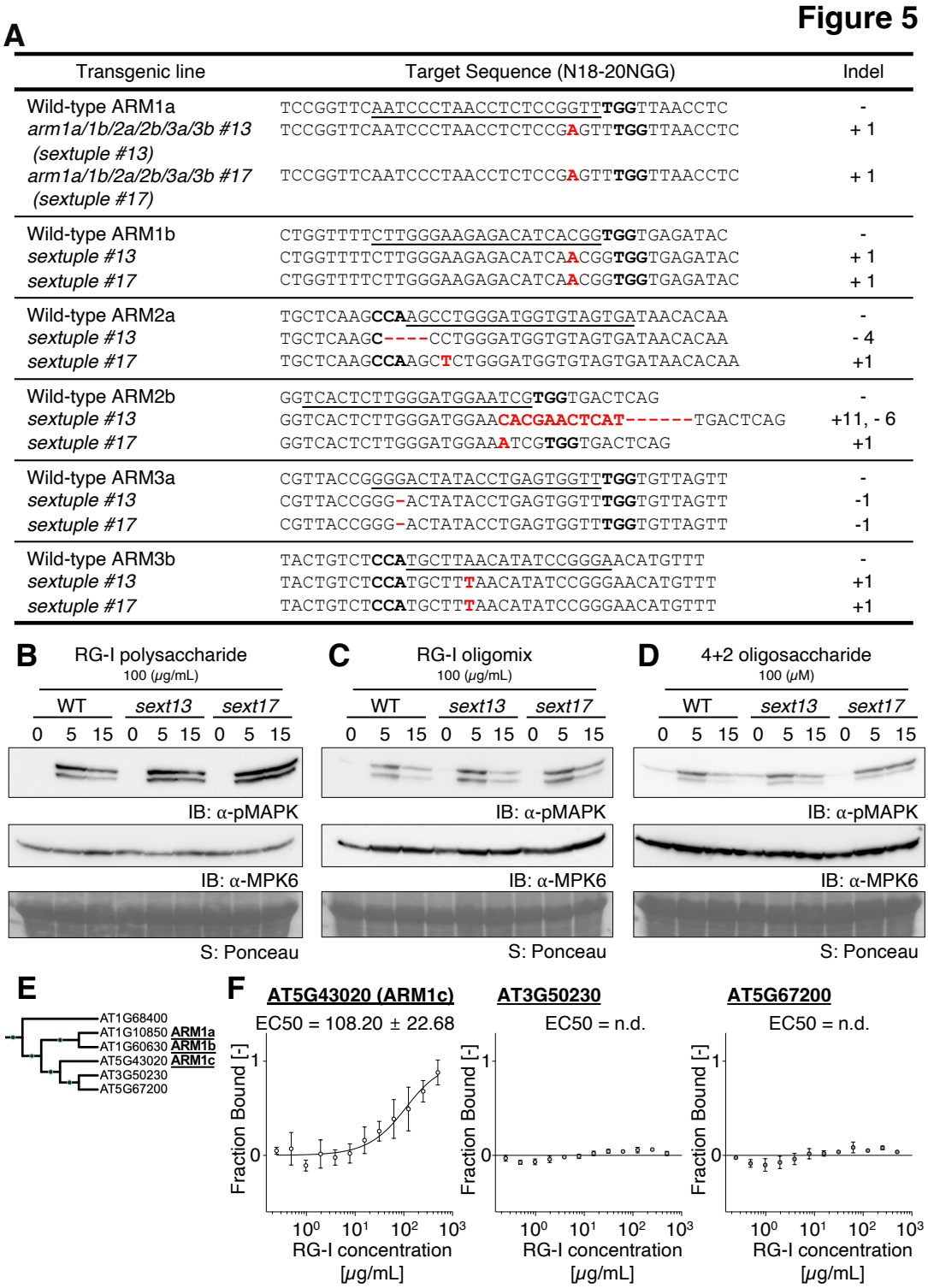

Fig. 5. ARM sextuple mutants showed similar MAPK activation in response to RG-I compared to wild-type and possible functional redundances with other receptors in RG-I-mediated immune responses.

A. Gene-editing mutations identified in the six *ARM* genes corresponding to the *arm1a/1b/2a/2b/3a/3c* sextuple mutants. **B-D.** Immunoblotting (IB) analyses of MAPK phosphorylation in wild-type (WT) and *arm* sextuple mutants Arabidopsis seedlings treated

with either RG-I or RG-I fragments. Treatment conditions, including concentrations and durations, are indicated at the top of the blots. This experiment was repeated twice with similar results. Equal loading of protein samples on the blot was controlled by anti-MPK blotting (middle) and Ponceau staining (bottom), which visualizes the Rubisco large subunit (rbcL). **E.** ARM1-containing clades from the receptor similarity tree. **F.** Quantification of interaction between RG-I polysaccharides and either ECDs of AT5G43020, AT3G50230, or AT5G67200 using MST. Data points in the fitted-dose response binding curves indicate the fraction of labeled ARM^{ECD} bound to each oligosaccharide as described (mean ± SE; AT5G43020, n=3; AT3G50230 and AT5G67200, n=4).

Fig. 6

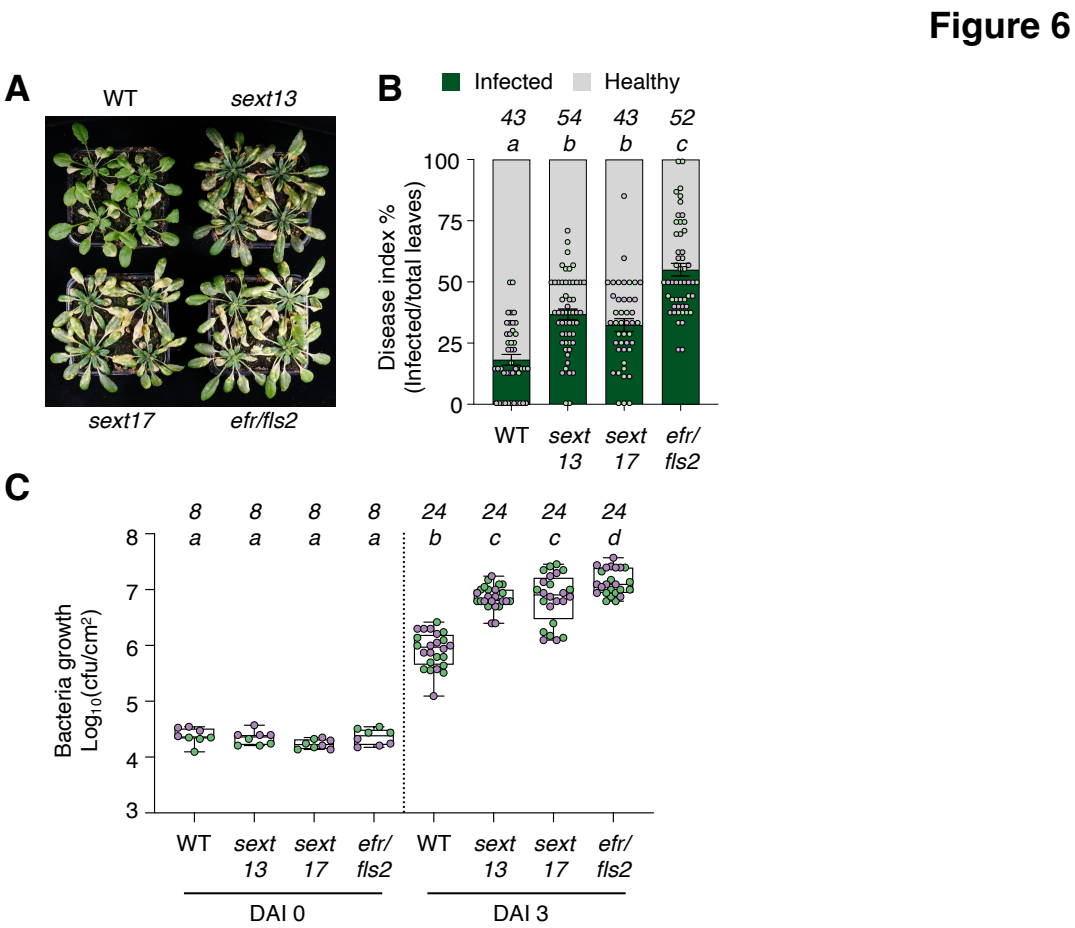

Fig. 6. ARM sextuple mutants showed a more susceptible phenotype against *Pseudomonas syringae pv. tomato* DC3000 infection than wild-type.

A. Representative pictures of Arabidopsis plants taken 5 days after inoculation with *Ps* DC3000. Genotypes are indicated at the top and bottom. **B.** The disease index percentage was calculated by dividing the number of infected leaves (more than half of the leaf being yellow) by the total number of leaves. The percentage of infected leaves is indicated with green, and that of healthy leaves is indicated with gray. Error bars indicate SE. **C.** Growth of *Ps* DC3000 in wild-type, *sextuple 13*, *sextuple 17*, *efr/fls2.* The number of bacteria per area of leaf (cfu/cm2) is plotted on a $\log_{10}$ scale for day after inoculation (DAI) 0 and DAI 3. The box plot represents the first and third quartiles, centered by the median, and whiskers extend to the minimum and maximum data points. **B and C.** Numbers of biologically independent observations (*n*) are indicated above the letters, and dots with different colors (green and purple dots) indicate different experimental trials. Letters above the boxes (a-d) indicate the results of statistical analysis using a linear mixed effect model with one-way ANOVA followed by a Tukey's multiple comparison test (two-sided, adjusted for multiple comparisons, $p < 0.05$).